Structure and stability of $Cd_2Nb_2O_7$ and $Cd_2Ta_2O_7$ explored by *ab initio* calculations

Michael Fischer,* Thomas Malcherek,† and Ulrich Bismayer
Mineralogisch-Petrographisches Institut, Universität Hamburg, Grindelallee 48, D-20146 Hamburg, Germany

Peter Blaha and Karlheinz Schwarz
Institute for Materials Chemistry, TU Wien, Getreidemarkt 9/165-TC, A-1060 Vienna, Austria

(Received 28 April 2008; published 17 July 2008)

Structural instabilities of $Cd_2Nb_2O_7$ have been explored by all-electron *ab initio* calculations in the framework of density-functional theory. The calculated phonon-dispersion curve of the cubic high-temperature phase displays several modes with imaginary frequencies. A distortion according to a T_{1u} mode at the Γ point leads to the energetically most favorable configuration. The resulting structure has been optimized in space-group symmetries *Ima*2 and *I*1*a*1 (*Cc*). The stability of these structures suggests a sequence of phase transitions $Fd\bar{3}m$-*Ima*2-*Cc*. The dominant structural changes occur as a result of the ferroelectric transition to orthorhombic symmetry, whereas the distortions associated with the subsequent transition to monoclinic symmetry are relatively small. With respect to the cubic phase, Nb is displaced most strongly. In both low-temperature phases, two crystallographically distinct Nb and Cd positions exist. The Nb displacements give rise to an ordered arrangement of short and long Nb-O bonds. In the *Ima*2 phase, chains of alternating long and short bonds propagate along [001] and along ⟨111⟩, while corresponding chains parallel to [100] still consist of symmetric Nb1-O bonds. The latter bonds distort only with the transition to the *Cc* phase. In contrast to $Cd_2Nb_2O_7$, the structure of $Cd_2Ta_2O_7$ returns to cubic symmetry when subjected to similar distortions.

DOI: 10.1103/PhysRevB.78.014108 PACS number(s): 77.80.−e, 71.15.Mb, 63.20.dk, 64.60.Ej

I. INTRODUCTION

Ferroelectricity in cadmium pyroniobate, $Cd_2Nb_2O_7$ (CNO), was discovered as early as 1952.[1] Since then the compound has attracted considerable interest because of its structural phase transitions and its unusual ferroelectric properties. However, to date neither the crystal structure of ferroelectric CNO nor the driving forces behind the ferroelectric transitions have been accurately determined.

Following recent reviews in Refs. 2 and 3 and references cited therein, the crystal structures and phase transitions (PTs) known to occur in CNO can be summarized as follows: Above $T_1=205$ K CNO is cubic, exhibiting the pyrochlore structure type in space-group (SG) symmetry $Fd\bar{3}m$. The pyrochlore structure is commonly described as composed of two interpenetrating networks without common constituents: The first network comprises linear O1-Cd-O1 bridges connected in a cuprite-type arrangement. The second network is formed by the Nb cations, which are sixfold coordinated by O2. The $[NbO_6]$ polyhedron is either an elongated or a compressed octahedron along the threefold axis, depending on the value of the only free structural parameter of the pyrochlore structure, x_{O2}. In the second coordination sphere, Cd is coordinated by six O2 atoms. On cooling below T_1, CNO transforms to a phase which is orthorhombic[4] or tetragonal.[5] The transition at T_1 is sometimes referred to as an improper ferroelastic[6] or an improper ferroelectric PT. Spontaneous polarization has been reported for all temperatures below T_1.[3] At $T_2=196$ K a proper ferroelectric (FE) transition occurs, evidenced by a polar soft mode.[4] A broad heat-capacity anomaly and a frequency dependent dielectric function[2] have been reported at and below T_2. The frequency dependence of the dielectric constant in this temperature regime is similar to that seen in typical relaxor materials, indicating the presence of polar clusters in CNO. While coupling of the FE mode to a central mode[4] has been proposed, other authors[7] saw the FE mode as an uncoupled but overdamped TO phonon mode. At $T_3\approx 85$ K a further structural PT has been observed, indicated by anomalies in heat capacity and dielectric constant. Below T_3 monoclinic symmetry has been proposed.[5] Some authors claimed that an incommensurate phase exists between T_3 and a further PT at $T_4=46$ K. Conclusive proof of such an incommensurate phase has not been presented yet. The occurrence of a PT near T_4 has been confirmed by heat-capacity measurements, however.[2]

Strongly anisotropic diffuse scattering has been observed in single crystals of CNO (Ref. 8) at ambient temperature. The diffuse scattering intensity is found in planes normal to $\langle 110\rangle_{cub}$, indicating local symmetry breaking with correlations along these directions.

Contrary to CNO, $Cd_2Ta_2O_7$ (CTO) is not ferroelectric. Just one phase transition has been reported at temperatures close to T_1, which might indicate that the corresponding phase transitions in CNO and in CTO are related.[9]

In spite of the abundant literature on dielectric properties of CNO, there is a remarkable lack of published crystallographic data and many of the available results differ substantially, highlighting the influence of impurities and defects. All low-temperature phases of CNO remain strongly pseudocubic; i.e., very little spontaneous strain is involved in the PTs. Diffraction studies of CNO thus remain difficult to interpret.[10] Here we report on the results of an *ab initio* study of CNO, thereby circumventing many of the problems inherent to previous experimental studies. The limitations of this computational approach include the neglect of possible disorder.[11]

II. METHODOLOGY

Total energies and interatomic forces were calculated using the (linearized) augmented plane wave plus local orbitals

method (L/APW+lo) implemented in the WIEN2K code.[12] The calculations were done using the generalized gradient approximation (GGA) exchange-correlation functional in the parametrization of Perdew *et al.*[13] A combination of APW +lo basis functions for the s,p,d states and LAPW basis for higher angular momenta[14] provided the best convergence. The core states were treated fully relativistically, whereas a scalar relativistic scheme was used for the valence states. Preliminary calculations ensured a good convergence of the quantities in question with respect to the Brillouin-zone (BZ) sampling and the cut-off parameter $R_{\mathrm{mt}}K_{\mathrm{max}}$ (the product of the smallest atomic sphere radius R_{mt} times the largest K vector in the plane-wave expansion). A mesh of eight k points in the full first BZ and $R_{\mathrm{mt}}K_{\mathrm{max}}=6$ was used for the frozen phonon calculations, as these values yielded well-converged interatomic forces. Subsequent optimization of the distorted structures was carried out with $R_{\mathrm{mt}}K_{\mathrm{max}}=7.5$ and 216 k vectors in the first BZ.

Attempts to optimize the volume of cubic CNO resulted in an overestimation of the equilibrium volume with respect to experimental values, a problem that is well known in DFT calculations using the GGA exchange-correlation functional.[15] Thus, the published experimentally determined lattice parameter $a=10.3665$ Å at $T=2$ K (Ref. 10) was used in all calculations, thereby arbitrarily setting the lattice strain to zero in all potential low-temperature (LT) phases. It is well known that the energy barrier for a displacive distortion in perovskites such as $KNbO_3$ and $KTaO_3$ is rather sensitive to volume.[16] In the present case, however, the experimentally detectable changes in volume and unit-cell shape at the ferroelectric phase transition are negligible. Keeping the experimental volume fixed is thus justified. A structure optimization for cubic CNO using the above lattice parameter led to an internal parameter $x_{\mathrm{O2}}=0.3193$. The resulting Nb-O2 bond length of 1.968 Å is in perfect agreement with the neutron-diffraction data of the cubic phase.[10]

In order to calculate the phonon-dispersion relation of CNO, the PHONON software was used.[17] This program employs the direct method to calculate the vibrational properties of crystals. It is based on the interatomic forces that are calculated for a set of structures. In each structure one atom is displaced in a certain direction and the corresponding force constants are derived from the resulting WIEN2K forces.[18]

The phonon-dispersion curves were calculated for the optimized cubic phase of CNO. The chosen supercell, i.e., the conventional unit cell of cubic CNO containing 88 atoms, was demonstrated to be of sufficient size since the calculated force constants for interatomic distances close to the length of the supercell had values close to zero. The phonon frequencies were calculated at five high-symmetry points of the first Brillouin zone and for 20 wave vectors in between each pair of adjacent high-symmetry points. A similar approach has already been applied to several other pyrochlore compounds.[19,20] The electric-field gradients (EFGs) have been obtained from the self-consistent charge density without further approximations as described in Ref. 21.

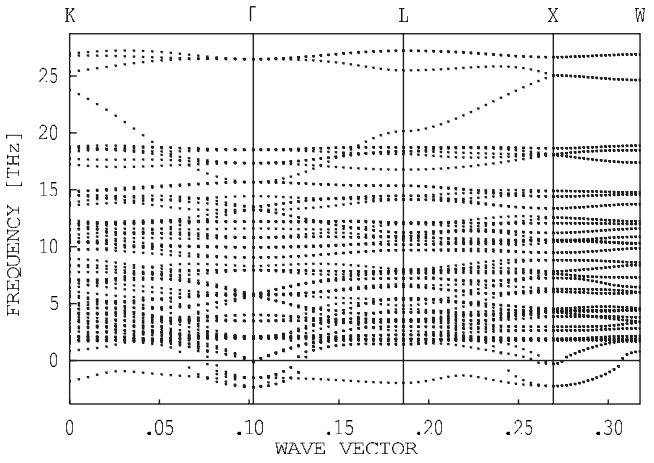

FIG. 1. Calculated phonon-dispersion curve for cubic CNO. The scale of the x axis corresponds to the modulus of the wave vector, starting from the K point.

III. RESULTS AND DISCUSSION

A. $Cd_2Nb_2O_7$

Structural instabilities throughout most of the Brillouin zone are evident in the phonon-dispersion curve (Fig. 1). The W point is the only point of high symmetry where all modes are stable, whereas there is more than one unstable mode each at the Γ and the X points.

In SG $Fd\bar{3}m$ there are eight infrared (IR)–active modes (T_{1u} symmetry) and four Raman-active modes (four T_{2g}, one A_{1g}, and one E_g). Concerning the six stable IR modes, good agreement between the calculated frequency values at the Γ point and the measured frequencies in Ref. 4 is observed (Table I). The high-frequency modes agree within a few percent, but the low-frequency modes are difficult to compare because they may be dominated by dynamical instabilities and anharmonic effects.

Concerning the Raman-active modes, the available experimental data[22,23] do not permit an unambiguous assignment to measured frequencies. This is caused by the presence of modes other than the six expected ones, indicating that some forbidden modes have to be active in CNO. In particular the strong bands at 588 and 637 cm^{-1} match the frequencies predicted for the T_{2u} and the T_{1g} modes, respectively (Table I), both of which are not nominally Raman active. The T_{2g} mode at 422 cm^{-1} has low intensity in both the high-pressure[23] and the ambient-pressure spectra.[22] The absence of the T_{2g} mode predicted at 883 cm^{-1} from the high-pressure data of Ref. 23 may be due to similar low intensity as well as the nonambient measurement conditions.

The most pronounced instabilities, represented by the most negative frequency values in Fig. 1, are a T_{1u} mode at the Γ point and a doubly degenerate mode at the X point. Two structures incorporating the atomic displacements corresponding to each of these two modes were generated. A distortion according to the T_{1u} mode led to a phase with $P1$ symmetry in a 22-atom cell (no cell multiplication). A distortion according to the mode at the X point led to a phase with $P2_12_12_1$ SG symmetry in a 44-atom cell (cell doubling).

TABLE I. Measured and calculated frequencies (in cm^{-1}) of stable modes at the Γ point. IR-active modes have been measured at $T=540$ K (Ref. 4). Raman mode frequencies have been measured at $T=290$ K (Ref. 22) and include several forbidden modes.

Expt.	Calc.	Irrep
	IR-active modes	
39	71	T_{1u}
87	116	T_{1u}
121	190	T_{1u}
350	360	T_{1u}
391	407	T_{1u}
535	523	T_{1u}
	Raman-active modes	
94	(69)	E_u [a]
158	(133)	E_u [a]
279	265	T_{2g}
313	302	E_g
339	332	T_{2g}
377	(387)	A_{2u} [a]
422	441	T_{2g}
509	482	A_{1g}
588	(579)	T_{2u} [a]
637	(617)	T_{1g} [a]
	883	T_{2g}

[a]Forbidden modes.

Both structures were optimized using the minimization procedure of the WIEN2K package. A symmetry search was carried out in both optimized structures using KPLOT.[24] With increasing tolerance, the $P1$ structure was found to be compatible with space groups Cc (No. 9) and $Ima2$ (No. 46). Both SG symmetries permit the observed ferroelectricity. Relating these results to the experimental observations in Ref. 5, the transition to the orthorhombic $Ima2$ phase corresponds to the ferroelectric transition at T_2, while the transition to the monoclinic Cc phase corresponds to the secondary transition at T_3.

Concerning the $P2_12_12_1$ phase, which is energetically less favorable, the compatible space groups are neither ferroelectric nor have they been observed experimentally. It can thus be concluded that, taking into account the limitations of the approach (assumption of a purely displacive transition and neglect of lattice strain), the *ab initio* calculations predict an unstable T_{1u} mode as the primary mode that drives the structural phase transitions. The other structural instabilities indicated by the phonon-dispersion relation (Fig. 1) might play a role as secondary modes and could be of particular importance for the transition at T_1.

The space groups $Ima2$ and Cc are isotropy subgroups of $Fd\bar{3}m$. Thus in principle an order parameter transforming according to an irreducible representation (Irrep) of $Fd\bar{3}m$ could explain the symmetry break $Fd\bar{3}m \rightarrow Ima2$ or $Fd\bar{3}m \rightarrow Cc$ in the context of a single continuous phase transition. Both the T_{1u} and the T_{2u} modes can produce the respective distorted phases, but only the T_{1u} mode is IR active.[4] The presence of several intermediate phases between $Fd\bar{3}m$ and Cc is indicative of competing order parameters. Figure 2 shows the chains of maximal subgroups between $Fd\bar{3}m$ and Cc. Candidate SG symmetries for the intermediate phase at T_1 would thus be $I4_1/amd$ or $Imma$, associated with the (Raman-active) modes E_g and T_{2g}, respectively. Both symmetries do not permit ferroelectricity, however, and would thus contradict the observed polarization below T_1.

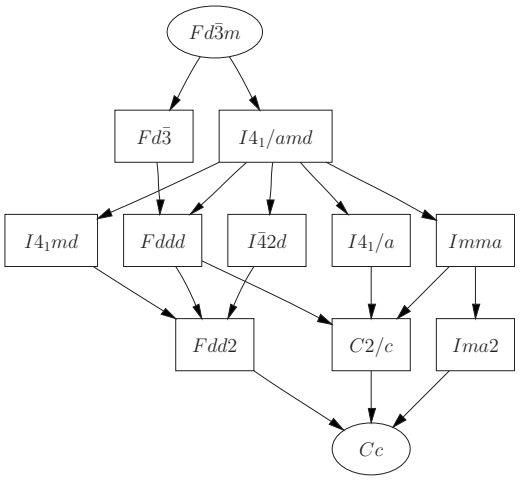

FIG. 2. Lattice of maximal subgroups (Ref. 25) for the SG pair $Fd\bar{3}m/Cc$ in the absence of cell multiplication.

The resulting two types of structures with symmetries $Ima2$ and Cc were again optimized. The Cc structure was transformed to an $I1a1$ setting in order to avoid a monoclinic angle of $\beta=135°$. As the lattice strain was neglected, this transformation results in an orthogonal cell, simplifying the comparison with the cubic and the orthorhombic structures. The origin of both LT phases was shifted along the polar directions in a way that the sum over all displacements in the respective direction becomes zero. The atomic positions of both phases are given in Table II and the $I1a1$ structure is shown in Fig. 3.

The differences in total energy between the two calculated LT phases and the cubic phase are given in Table III. It is apparent that the main change in total energy occurs at the transition from the cubic phase to the orthorhombic phase, the $Ima2$ phase being energetically favored by 1.004 kJ/mol. In comparison, the further change in total energy at the transition to the monoclinic phase is rather small, amounting to 0.091 kJ/mol. According to the experimentally determined excess entropies for the phase transitions at T_2 and T_3,[2] the expected values would be 0.4 and 0.01 kJ/mol, respectively. The discrepancies might be related to the chosen base lines in the determination of the transition entropies, or they might indicate possible order-disorder contributions to the phase transitions in CNO.

Calculated EFG parameters at the various atomic sites are given in Table IV. Perturbed angular correlation measurements of CNO (Ref. 26) confirm two Cd sites at low temperatures. Based on the measured quadrupole coupling frequencies in Ref. 26 and a nuclear quadrupole moment of 7.8×10^{-29} m^2 for ^{111}Cd,[27] the respective moduli of V_{zz} are 17.08×10^{21} and 16.54×10^{21} V m^{-2} for the distorted phase

TABLE II. Structural parameters of calculated LT phases with *Ima*2 and *I*1*a*1 symmetries. Both structures are set in identical 44-atom cells, i.e., $Z=4$. The lattice parameters (in Å) of both phases are $a=7.3295$, $b=10.3655$, and $c=a$ with orthogonal axes. The corresponding pseudocubic cell has $a_{cub}=b$. WP=Wyckoff position.

		*Ima*2 phase					*I*1*a*1 phase		
Atom	WP	*x*	*y*	*z*	Atom	WP	*x*	*y*	*z*
Cd1	4*a*	0	0	0.5078	Cd1	4*a*	−0.0002	0.0004	0.5071
Cd2	4*b*	0.25	0.2535	0.2525	Cd2	4*a*	0.2482	0.2537	0.2521
Nb1	4*a*	0	0	0.0076	Nb1	4*a*	−0.0031	0.0004	0.0080
Nb2	4*b*	0.25	0.7453	0.2633	Nb2	4*a*	0.2489	0.7449	0.2625
O1	4*b*	0.25	0.3746	−0.0015	O1	4*a*	0.2504	0.3747	−0.0019
O2	4*b*	0.25	0.8207	0.4992	O2	4*a*	0.2511	0.8208	0.4988
O3	4*b*	0.25	0.0688	−0.0072	O3	4*a*	0.2500	0.0686	−0.0063
O4	8*c*	0.9467	0.1241	0.8002	O4	4*a*	0.9476	0.1245	0.8007
O5	8*c*	0.9419	0.3736	0.6890	O5	4*a*	0.0596	0.6263	0.6885
					O6	4*a*	0.9437	0.3733	0.6902
					O7	4*a*	0.0537	0.8761	0.8003

and 16.37×10^{21} V m^{-2} for the cubic phase of CNO. The observed asymmetry parameter is zero. Considering the uncertainty of the quadrupole moment and the neglected finite temperature effects, the calculated $|V_{zz}|$ in Table IV agree reasonably well with these experimental results.

Compared to the cubic phase, both [NbO_6] octahedra of the LT phases show a considerable degree of distortion (Fig. 4). The changes in Nb-O bond lengths are caused mainly by a displacement of the central cations toward octahedron edges ([$Nb1O_6$]) or faces ([$Nb2O_6$]). The displacements with respect to the cubic phase amount to 0.056 Å for Nb1 and 0.109 Å for Nb2. However, the oxygen framework surrounding the niobium atoms is also affected: The displacements of the oxygen atoms range from 0.015 Å for O2 to 0.053 Å for O3, and in some cases, a considerable deviation of the O-O distances from the cubic values is observed.

Considering the [CdO_8] polyhedra in the *Ima*2 phase, it is notable that the Cd-O1 distances remain practically identical to the cubic value of 2.244 Å, in spite of the fact that both Cd atoms are displaced considerably: The Cd1 atom is shifted by 0.057 Å and the Cd2 atom by 0.040 Å with respect to the cubic phase. The distances between Cd and the oxygen atoms that are coordinated to Nb in the first coordination sphere deviate quite strongly from the cubic value of 2.620 Å, ranging from 2.530 to 2.713 Å. The distortion of the Nb sublattice is small in comparison to that in $Y_2Nb_2O_7$,[19] with only minor deviations of the Nb-Nb distances from the cubic value. In comparison to the displacements described above, the additional displacements associated with the transition to the monoclinic phase are small, and the coordination polyhedra remain very similar to those of the orthorhombic phase.

In the *Ima*2 phase, all cations are displaced from their cubic position along the same direction parallel to [001], whereas all anions are displaced along the opposite direction: The resulting dipole moment of each unit cell is consistent with the macroscopic ferroelectricity. As [001] of the orthorhombic phase corresponds to [110] of the cubic phase, this orientation of the polarization would lead to a formation of ferroelectric domains along $[110]_{cub}$, which are indeed observed experimentally.[6] In the monoclinic phase, there is an additional component of displacement along [100]. Again, cations and (most) anions are shifted in opposite directions along this axis. Thus, the polarization vector has the direction $[h0l]$, corresponding to $[hk0]_{cub}$.

The displacements and the resulting direction of polarization can be seen in a different way that emphasizes the chain components of the pyrochlore structure: The *Ima*2 phase exhibits ordered chains of corner sharing octahedra, in the sense that short (1.898 Å) and long (2.052 Å) Nb-O bonds alternate parallel to [001] [Fig. 3(a)]. A similar alternation of long and short Nb-O bonds is found parallel to ⟨111⟩. In these directions Nb1 and Nb2 alternate as well; thus two different short bonds (1.931 and 1.915 Å) and two different long bonds (2.029 and 2.011 Å) occur. No such alternation is found parallel to [100] with the Nb1-O3 bond (1.969 Å) connecting the octahedra in chain direction. However, this remaining symmetry is lifted in the *Cc* phase, where the alternation of long and short bonds is also attained along [100]. The associated distortion is small though and the long and short bond distances in this direction do not differ much [1.988 and 1.949 Å; Fig. 3(b)].

Bond valence calculations were carried out for the cubic phase and both calculated LT phases using the program SOFTBV, employing "bond softness" parameters.[28] The main results are included in Table III. The calculations reveal a drastic underbonding of Cd and O1 and a less significant overbonding of Nb in cubic CNO. In the LT phases, the situation improves slightly, but there are no drastic changes in the calculated bond valence sums. The empirical bond strain as measured by the global instability index G_{ii} is at the upper limit (0.2) of what is considered tolerable for a stable structure.[29,30] This critical value slightly relaxes on distortion to the orthorhombic and monoclinic structures (Table III). The decrease in the global instability index in the LT phases correlates with the decrease in the total energy obtained in the *ab initio* calculations.

An overview of the density of states (DOS) of cubic CNO close to the Fermi energy E_F is shown in Fig. 5. The obtained

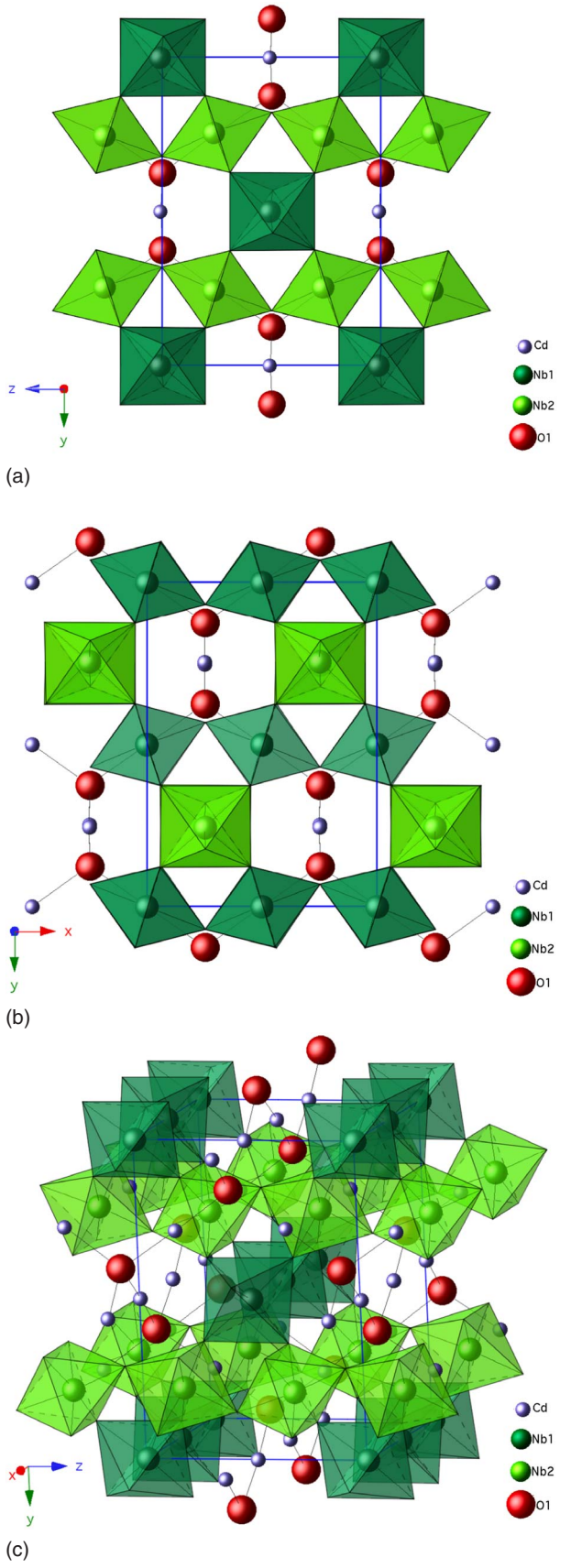

FIG. 3. (Color online) The $I1a1$ structure projected along [100] (a) and along [001] (b) and in tilted view (c). The O2 atoms are located at the corners of the octahedra.

TABLE III. Some calculated quantities for optimized LT phases and cubic pyrochlore structure of CNO. ΔE corresponds to the difference in total energy with respect to the cubic phase. For Cd, Nb, and O2, the bond valence sums V_i [given in valence units (v.u.)] of the LT phases are averaged over the respective nonequivalent atoms. The global instability index G_{ii} is calculated according to $G_{ii}^2=N^{-1}\Sigma_{i=1}^{N}(V_i-V_i^0)^2$, where V_i^0 is the formal valence sum.

	$Fd\bar{3}m$	$Ima2$	$I1a1$
Assumed range of stability	$T>T_2$	$T_2>T>T_3$	$T_3>T$
ΔE (Ry/primitive cell)		-1.529×10^{-3}	-1.667×10^{-3}
ΔE (kJ/mol)		−1.004	−1.094
V_i(Cd) (v.u.)	1.667	1.678	1.679
V_i(Nb) (v.u.)	5.120	5.114	5.112
V_i(O1) (v.u.)	1.569	1.568	1.567
V_i(O2) (v.u.)	2.000	2.003	2.002
G_{ii}	0.1992	0.1954	0.1951

DOS in the cubic phase is in good qualitative agreement with previous calculations for cubic CNO.[31] The DOS clearly reproduces the insulating character of CNO. The energy ranges of interest for the chemical bonding were inspected in detail, using partial DOS plots and energy-resolved electron-density maps (Fig. 6). With increasing energy, the following peak manifolds can be distinguished, as labeled in Fig. 5: (A) O2 2*s* states interact with Nb 4*d* states, indicated by a slight increase in the Nb partial DOS as well as a nonzero electron density along the Nb-O2 bond. A narrow O1 contribution appears at the upper edge of the manifold. (B) Cd 4*d* states mainly contribute to the peak at −6 eV. The electron-density map in this energy range reveals a considerable electron density between Cd and O1, indicating some covalent contribution to the bond. The interaction of Cd with the more distant O2 atoms is much weaker. (C) The energy range near −4 eV corresponds to the Nb-O bonding. Both O2 2*p* states and Nb 4*d* states contribute considerably to the bonding. An electron-density map of this energy region reveals a strong anisotropy of the Nb-O2 bonds. The bonding situation is similar to other Nb oxide ferroelectrics, e.g., $LiNbO_3$,[32] which show a high polarizability of the Nb-O bonds. (D) The peaks directly below E_F comprise those oxygen 2*p* states that do not take part in the bonding. Almost all O1 *p* character is localized in this narrow DOS structure. In the unoccupied region, nonbonding *d* states of Nb (E) and Nb-O antibonding states (G) as well as a Cd-O antibonding peak state (F), can be identified.

The DOS plots of the LT phases do not exhibit any remarkable differences in comparison with cubic CNO. However, the fact that the peaks are broader is clearly related to the less regular coordination environment of the atoms. As the main geometrical changes occur within the $[NbO_6]$ octahedra, only the electron-density maps of the energy range of Nb-O bonding differ considerably from those of the cubic case: The electron density increases along those bonds that are shortened with respect to cubic CNO, whereas it decreases for those bonds that are elongated. In the latter case, enhanced electron density appears at the e_g orbital lobes closer to Nb (Fig. 6). As the minimal electron density along

TABLE IV. Calculated electric-field gradients of CNO and CTO. Principal components V_{zz} are given in 10^{21} V m^{-2}.

	$Fd\bar{3}m$			*Ima*2			*I*1*a*1	
Atom	V_{zz}	η	Atom	V_{zz}	η	Atom	V_{zz}	η
Cd	−14.16	0.0	Cd1	−13.81	0.0	Cd1	−13.85	0.01
			Cd2	−14.22	0.0	Cd2	−14.18	0.01
Nb	4.34	0.0	Nb1	3.62	0.29	Nb1	3.73	0.35
			Nb2	6.05	0.01	Nb2	6.08	0.05
O1	0.0	0.0	O1	0.22	0.12	O1	0.22	0.41
O2	−1.02	0.72	O2	−1.71	0.78	O2	−1.63	0.83
	CTO		O3	0.86	0.87	O3	0.92	0.96
Cd	−14.28	0.0	O4	−1.11	0.55	O4	−0.97	0.53
Ta	10.35	0.0	O5	1.38	0.80	O5	1.38	0.95
O1	0.0	0.0				O6	1.38	0.95
O2	0.83	0.37				O7	−1.26	0.60

the length of the bond is significantly larger for the Nb-O2 bonds than for the Cd-O1 bonds, it can be concluded that the Nb-O bonding has a larger covalent contribution than the Cd-O bonding.

Due to the fact that these are the most notable changes in valence electron distribution in the LT phases, it can be concluded that the interaction between Nb 4*d* states and O2 *p* states is of crucial importance for the structural distortion associated with the phase transition: It is the environment of Nb that becomes energetically unstable on cooling, leading to a distortion of the [NbO_6] octahedron, thereby triggering the structural phase transition.

B. $Cd_2Ta_2O_7$

The *P*1 structure of CNO generated above was modified by replacing Nb with Ta. A subsequent geometry optimization returned to the cubic pyrochlore structure within a close tolerance. Thus the *ab initio* calculations indicate that $Cd_2Ta_2O_7$ (CTO) does not form the same low-temperature structure as CNO, but we have not searched systematically for other instabilities. The Ta-O2 bond length of optimized CTO amounts to 1.969 Å and is practically identical to the corresponding distance of the niobate. Bond valence calculations for cubic CTO show deviations from the nominal valences that are very close to those calculated for cubic CNO. In contrast to CNO, the resulting bond strain remains unrelaxed in CTO. As in experiment[26] there is little variation

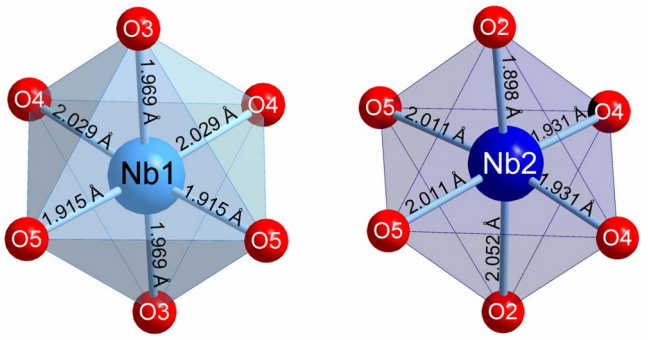

FIG. 4. (Color online) Graphical representation of nonequivalent NbO_6 octahedra of the *Ima*2 phase, including Nb-O bond lengths. The $Nb1O_6$ octahedra are connected via the O3 atoms and form chains parallel to [100]; the $Nb2O_6$ octahedra are connected via the O2 atoms and form chains parallel to [001]. The atoms O4 and O5 connect octahedra of different types.

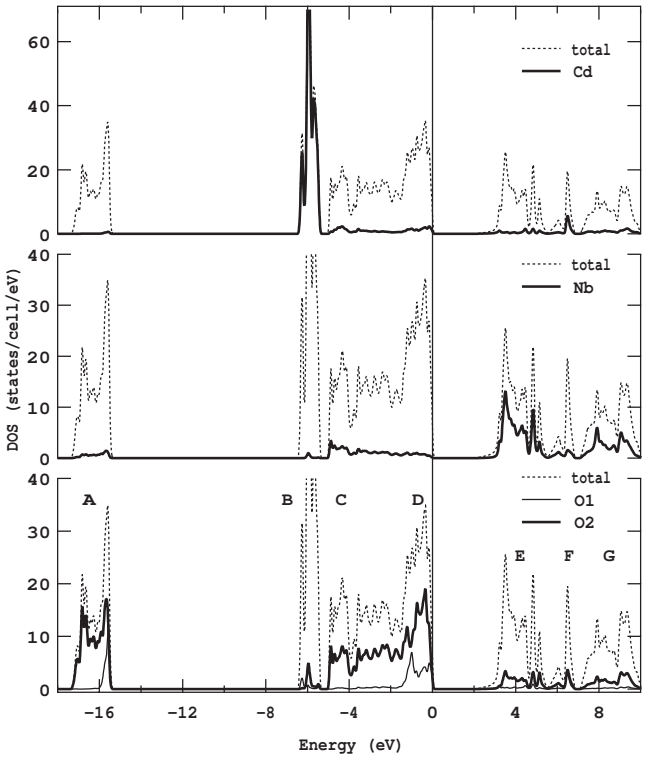

FIG. 5. Electronic density of states of cubic CNO (dashed line) close to the Fermi energy (E_F=0 eV). The solid lines show the contributions of Cd, Nb, and O in the top, middle, and bottom diagrams, respectively.

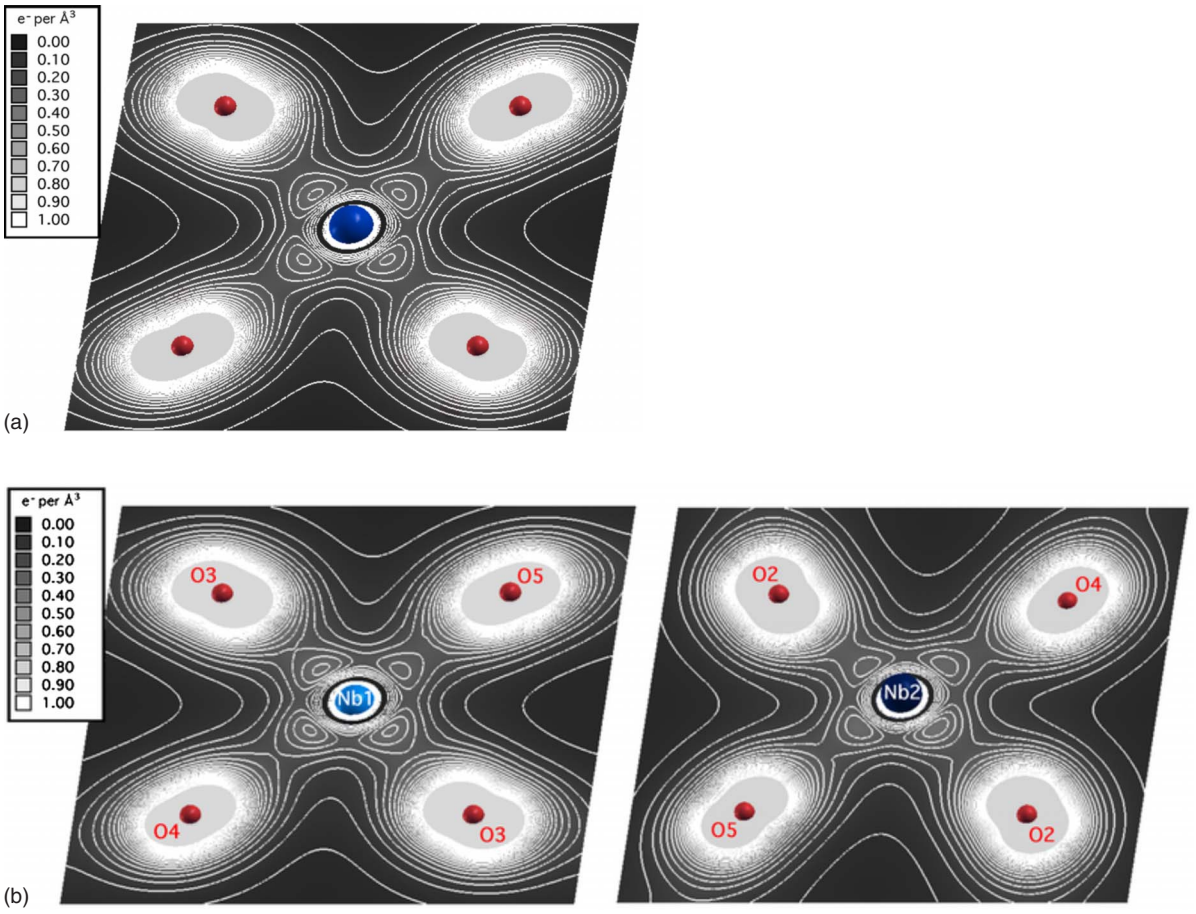

FIG. 6. (Color online) Electron-density maps for the energy region of Nb-O *d-p* bonding (−5.55 eV$<E<$−2.83 eV) in the $Fd\bar{3}m$ phase (a) and in the *Ima*2 phase (b). Isolines are in equal steps of $\approx 0.05e$ Å^{-3}.

in the Cd-EFG parameters between CNO and CTO (Table IV).

The calculated density of states of cubic CTO is quite similar to the one shown in Fig. 5, but it exhibits an additional peak at −18 eV, corresponding to the occupied Ta 4*f* states. Energy-resolved electron-density maps reveal an increased interaction of the O 2*s* states with the Ta 5*d* and 4*f*-states as compared to the O2 *s*-Nb *d* interaction in CNO. The interaction of Ta states with the O2 2*p* states is slightly diminished with respect to CNO, and the electron-density map shows that the *d-p* bonds are somewhat more diffuse and less directional, which can be related to the relativistic expansion of the 5*d* orbitals.[33] It can be assumed that these differences in electronic structure are directly connected to the increased stability of CTO: Due to the lesser degree of covalence of the Ta-O bonds, distortion of the $[TaO_6]$ octahedron does not yield an energetic benefit as in CNO; thus the phase transition does not occur. It is a typical feature of many isostructural niobate-tantalate pairs that the niobate compound undergoes structural phase transitions on cooling, whereas the tantalate compound does not. A well-known example is the pair $KNbO_3/KTaO_3$: While potassium niobate exhibits numerous phase transitions and ferroelectric behavior on cooling, potassium tantalate remains cubic down to low temperatures, although a soft phonon mode and incipient ferroelectricity indicate the presence of a structural instability.[33]

IV. CONCLUSIONS

The pyrochlore structured compounds CNO and CTO represent a typical example of the dichotomy between ferroelectric niobates on one hand and incipient ferroelectric tantalates on the other. However, it is well known that the ferroelectric transitions in $KNbO_3$ involve a significant degree of order-disorder character.[34] The evident local symmetry breaking, indicated by the observed diffuse scattering, suggests that a similar order-disorder component might also be involved in CNO. The present calculations show that a purely displacive ground state of CNO is characterized by a three-dimensional network of alternating short and long Nb-O bonds. However, in the presence of multiple-well ordering, geometrical frustration on the pyrochlore lattice might inhibit the formation of the fully ordered ferroelectric ground-state structure of CNO. Further studies are currently under way to elucidate these aspects.

ACKNOWLEDGMENTS

The authors would like to thank J. M. Perez Mato and B. Mihailova for useful discussions. Financial support by the German Research Foundation (DFG) was provided under Grant No. MA2284/3-1. M.F. acknowledges support by the German National Merit Foundation.

*Present address: Institut für Anorganische u. Angewandte Chemie, Universität Hamburg, Martin-Luther-King-Platz 6, D-20146 Hamburg, Germany.
†thomas.malcherek@uni-hamburg.de

[1] W. R. Cook and H. Jaffe, Phys. Rev. **88**, 1426 (1952).
[2] M. Tachibana, H. Kawaji, and T. Atake, Phys. Rev. B **70**, 064103 (2004).
[3] V. A. Isupov, Phys. Solid State **47**, 2119 (2005).
[4] E. Buixaderas, S. Kamba, J. Petzelt, M. Savinov, and N. N. Kolpakova, Eur. Phys. J. B **19**, 9 (2001).
[5] A. Küster, *Phasenübergänge bei ferroelektrischem $Cd_2Nb_2O_7$ und verwandten Substanzen* (Dissertationsschrift, Tübingen, Germany, 1992).
[6] N. N. Kolpakova, S. Waplak, and W. Bednarski, J. Phys.: Condens. Matter **10**, 9309 (1998).
[7] G. A. Samara, E. L. Venturini, and L. A. Boatner, J. Appl. Phys. **100**, 074112 (2006).
[8] T. Malcherek, J. Phys.: Condens. Matter **19**, 275208 (2007).
[9] A. W. Sleight and J. D. Bierlein, Solid State Commun. **18**, 163 (1976).
[10] M. T. Weller, R. W. Hughes, J. Rooke, C. S. Knee, and J. Reading, Dalton Trans. **2** (19), 3032 (2004).
[11] The often cited occurrence of dynamic Cd disorder (Ref. 35) in CNO is debatable. If the temperature dependence of thermal displacement parameters is used to deduce such disorder (site splitting), the results given in the reference support Nb rather than Cd disorder if properly extrapolated to 0 K.
[12] P. Blaha, K. Schwarz, G. K. H. Madsen, D. Kvasnicka, and J. Luitz, *WIEN2k, An Augmented Plane Wave Plus Local Orbitals Program for Calculating Crystal Properties* (Karlheinz Schwarz, Technische Universitat Wien, Austria, 2001).
[13] J. P. Perdew, K. Burke, and M. Ernzerhof, Phys. Rev. Lett. **77**, 3865 (1996).
[14] G. K. H. Madsen, P. Blaha, K. Schwarz, E. Sjöstedt, and L. Nordström, Phys. Rev. B **64**, 195134 (2001).
[15] Z. Wu and R. E. Cohen, Phys. Rev. B **73**, 235116 (2006).
[16] A. V. Postnikov, T. Neumann, G. Borstel, and M. Methfessel, Phys. Rev. B **48**, 5910 (1993).
[17] K. Parlinski, PHONON—software version 4.24, supplied users guide version 3.11, 2002; see http://wolf.ifj.edu.pl/phonon/
[18] K. Parlinski, Z. Q. Li, and Y. Kawazoe, Phys. Rev. Lett. **78**, 4063 (1997).
[19] P. Blaha, D. J. Singh, and K. Schwarz, Phys. Rev. Lett. **93**, 216403 (2004).
[20] I. A. Sergienko *et al.*, Phys. Rev. Lett. **92**, 065501 (2004).
[21] P. Blaha, K. Schwarz, W. Faber, and J. Luitz, Hyperfine Interact. **126**, 389 (2000).
[22] N. N. Kolpakova, M. Wiesner, G. Kugel, and P. Bourson, Ferroelectrics **190**, 179 (1997).
[23] F. X. Zhang, J. Lian, U. Becker, R. C. Ewing, L. M. Wang, L. A. Boatner, J. Hu, and S. K. Saxena, Phys. Rev. B **74**, 174116 (2006).
[24] R. Hundt, J. C. Schön, A. Hannemann, and M. Jansen, J. Appl. Crystallogr. **32**, 413 (1999).
[25] S. Ivantchev, E. Kroumova, G. Madariaga, J. M. Pérez-Mato, and M. I. Aroyo, J. Appl. Crystallogr. **33**, 1190 (2000).
[26] Y. Ohkubo, Y. Murakami, T. Saito, A. Yokoyama, and Y. Kawase, Mater. Trans. **45**, 1998 (2004).
[27] P. Pyykkö, Mol. Phys. **99**, 1617 (2001).
[28] S. Adams, SOFTBV version 0.96, 2007, http://kristall.uni-mki.gwdg.de/softbv/
[29] I. D. Brown, *The Chemical Bond in Inorganic Chemistry—The Bond Valence Model* (Oxford University Press, Oxford, 2002).
[30] I. Etxebarria, J. M. Perez-Mato, A. Garcia, P. Blaha, K. Schwarz, and J. Rodriguez-Carvajal, Phys. Rev. B **72**, 174108 (2005).
[31] R. Terki, G. Bertrand, H. Aourag, and C. Coddet, Physica B (Amsterdam) **392**, 341 (2007).
[32] I. Inbar and R. E. Cohen, Phys. Rev. B **53**, 1193 (1996).
[33] M. Kaupp, Angew. Chem., Int. Ed. **40**, 3534 (2001).
[34] R. Comes, M. Lambert, and A. Guinier, Solid State Commun. **6**, 715 (1968).
[35] K. Lukaszewicz, A. Pietraszko, J. Stepiendamm, and N. N. Kolpakova, Mater. Res. Bull. **29**, 987 (1994).